6 Multi-Orbital Cluster Perturbation Theory for Transition-Metal Oxides

Franca Manghi
Dipartimento di Fisica, Informatica e Matematica
University of Modena and Reggio Emilia, Italy

Contents

E. Pavarini, E. Koch, J. van den Brink, and G. Sawatzky (eds.)
Quantum Materials: Experiments and Theory
Modeling and Simulation Vol. 6
Forschungszentrum Jülich, 2016, ISBN 978-3-95806-159-0
http://www.cond-mat.de/events/correl16

1 Introduction

Electrons in solids behave in most cases like independent particles, and that in spite of the strong interactions between them. The explanation of this apparent paradox relies on the concept of the Landau quasi-particle: the multiple forces acting on one electron dress it up with an interaction cloud and these new dressed particles (quasi-particles) are effectively independent one from the other. The time evolution of the system with one electron removed is what is measured in experiments and when this state evolves as a coherent superposition of oscillations of approximately the same frequency it corresponds to the propagation of a quasi-particle with a reasonably well defined energy and a sufficiently long life-time. In this situation the low-energy excitations of the interacting electrons can be put into a one-to-one correspondence with those of non-interacting electrons with renormalized properties (energy and mass) and the measured spectra can be reduced to a quasi-particle band structure.

From a theoretical point of view, the simplest way to account for the electron-electron interaction is to include it as a mean field, where each electron moves independently under the influence of the average charge distribution of all the others. Materials for which this rudimentary mean-field description is sufficient have broad energy bands associated with large values of the electron kinetic energy. This implies that the electrons are highly itinerant and therefore it is reasonable to describe them using a picture in which interactions become smooth and can be averaged over. On the contrary when bands are narrower and the associated kinetic energy smaller, namely when electrons tend to localize around lattice ions, they see each other as individual point charges and the correlation between their motion becomes important. For these systems the single-particle picture is inadequate and their electronic properties have to be described including the multiple pair-wise e-e interaction as a true many-body term.

Strongly correlated electron systems have been one of the most important topics in theoretical solid state research for more than half a century. The major challenge is that the interesting physics occurs in the regime of intermediate coupling strength, where perturbation theory does not apply. The search for non perturbative approaches has been intense in the last decades, leading to some widely accepted results, the most prominent one being the choice of the Hubbard model as the general framework to describe strong e-e correlation.

A variety of non-perturbative techniques have been proposed during the years to tackle this problem, ranging from Dynamical Mean Field Theory (DMFT) [1] to 3-Body Scattering (3BS) theory [2, 3]. However the agreement between experiments and many-body calculations is still far from being fully quantitative [4–6] and different theoretical methods are constantly explored.

Recently schemes based on cluster formalisms have been developed. These so-called Quantum Cluster (QC) theories [7] share the basic idea to solve the problem of many interacting electrons in an extended lattice by a *divide-and-conquer* strategy, namely solving first the many-body problem in a subsystem of finite size and then embedding it within the infinite medium. The embedding procedure can be variationally optimized as in the Dynamical Cluster Approach (DCA) [8] and Cellular Dynamical Mean Field Theory (CDMFT) [9]. Even neglecting optimization in the embedding procedure the method, that in this case has been called Cluster

Perturbation Theory (CPT) [10], gives access to non trivial many-body effects, reproducing exactly both the non-interacting band limit and the atomic limit when on-site repulsion exceeds intersite hopping; for intermediate values of on-site e-e repulsion CPT opens a gap in metallic systems at half occupation. QC approaches account for the momentum dependence of many-body corrections more appropriately than other schemes, and for this reason they should provide a more accurate description of the quasi-particle dispersion. However QC approaches have been mostly applied to model systems and only few quasi-particle calculations for realistic systems have been reported up to now [11, 12]. The application of CPT to multi-orbital solids and to transition-metal oxides in particular will be our focus.

2 CPT for multiorbital systems

In CPT the lattice is seen as a periodic repetition of identical clusters and the Hubbard Hamiltonian can be partitioned in two terms, an intra-cluster ($\hat{H}_c$) and an inter-cluster one ($\hat{V}$)

$$\hat{H} = \hat{H}_c + \hat{V}\,, \tag{1}$$

where

$$\begin{aligned} \hat{H}_c &= \sum_{il\alpha} \varepsilon_{il\alpha}\,\hat{n}_{il\alpha} + \sum_{\alpha\beta}\sum_{ijl} t_{il\alpha,jl\beta}\,\hat{c}^{\dagger}_{il\alpha}\hat{c}_{jl\beta} + \sum_{il\alpha\beta} U^{i}_{\alpha\beta}\,\hat{n}_{il\alpha\uparrow}\hat{n}_{il\beta\downarrow} \\ \hat{V} &= \sum_{\alpha\beta}\sum_{ij,l\neq l'} t_{il\alpha,jl'\beta}\,\hat{c}^{\dagger}_{il\alpha}\hat{c}_{jl'\beta}\,. \end{aligned} \tag{2}$$

Here α, β are orbital indices, $\varepsilon_{il\alpha}$ are intra-atomic orbital parameters and $t_{il\alpha,jl'\beta}$ hopping terms connecting orbitals centered on different sites. Each atom is identified by the cluster it belongs to (index l) and by its position inside the cluster (index i). The lattice is a collection of $L \to \infty$ clusters each of them containing M atoms whose position is identified by the vector $\mathbf{R}_l$+$\mathbf{r}_i$. Each atom in the cluster is characterized by a set of orbitals $n_i^{\rm orb}$ per site and $K = \sum_{i=1}^{M} n_i^{\rm orb}$ is the total number of orbitals per cluster.

Since in the Hubbard model the e-e Coulomb interaction is on-site, the inter-cluster Hamiltonian $\hat{V}$ contains only single-particle terms and the many-body part is present in the intra-cluster Hamiltonian $\hat{H}_c$ only. Of course the complexity of the problem resides in the coexistence of the two contributions, while in the two limits $t \gg U$ or $U \gg t$ the Hamiltonian can be easily solved: in the first case the many-body term is negligible and $\hat{H}$ is reduced to a trivial one-body Hamiltonian; the second case, the atomic limit, corresponds to $\hat{H} \simeq \hat{H}_c$, namely to a Hamiltonian that does not mix the coordinates of electrons belonging to different clusters. In this case the eigenstates $|\Psi_n^N\rangle$ of the full Hamiltonian for N electrons ($N =\to \infty$) becomes

$$|\Psi_n^N\rangle = |\Phi_n^N\rangle = \prod_{l=1}^{L\to\infty} |\phi_n^K(l)\rangle \tag{3}$$

where $|\phi_n^K(l)\rangle$ are the few-body eigenstates of the l-th isolated cluster that can be calculated numerically by exact diagonalization.

The partition of the Hamiltonian into intra-cluster and inter-cluster terms gives rise to some exact expressions and suggests some relevant approximations. Let us consider the resolvent operator $\hat{G}$

$$\hat{G}^{-1}(z) \equiv z - \hat{H}_c - \hat{V} = \hat{G^c}^{-1} - \hat{V} \quad \text{with} \quad \hat{G^c}^{-1} \equiv z - \hat{H}_c \tag{4}$$

and the Dyson-like equation that is deduced from it $\hat{G} = \hat{G^c} + \hat{G^c}\,\hat{V}\,\hat{G}$, where the lattice Green function and the cluster one are connected by the inter-cluster interaction. The expectation value of the resolvent operator over the interacting ground state with one removed/added particle, $\hat{c}_{\mathbf{k}n}|\Psi_0^N\rangle$ / $\hat{c}^\dagger_{\mathbf{k}n}|\Psi_0^N\rangle$, gives the one-particle propagator for the extended lattice

$$\mathcal{G}(\mathbf{k}n\omega) = \mathcal{G}^+(\mathbf{k}n\omega) + \mathcal{G}^-(\mathbf{k}n\omega) \tag{5}$$

with $\mathcal{G}^\pm(\mathbf{k}n\omega)$, the particle and hole propagators, given by

$$\begin{aligned} \mathcal{G}^-(\mathbf{k}n\omega) &= \langle\Psi_0^N|\,\hat{c}^\dagger_{\mathbf{k}n}\,\hat{G}(-\omega + E_0^N + i\eta)\,\hat{c}_{\mathbf{k}n}\,|\Psi_0^N\rangle \\ \mathcal{G}^+(\mathbf{k}n\omega) &= \langle\Psi_0^N|\,\hat{c}_{\mathbf{k}n}\,\hat{G}(\ \ \omega + E_0^N + i\eta)\,\hat{c}^\dagger_{\mathbf{k}n}\,|\Psi_0^N\rangle\,. \end{aligned} \tag{6}$$

Since we are looking for a relationship between the lattice and cluster Green function, it is useful to introduce a transformation from the localized to the Bloch basis

$$\hat{c}_{\mathbf{k}n} = \frac{1}{\sqrt{K\times L}}\sum_{il\alpha}\mathcal{C}^n_{i\alpha}(\mathbf{k})e^{i\mathbf{k}\cdot(\mathbf{R}_l+\mathbf{r}_i)}\,\hat{c}_{il\alpha} \quad \text{and} \quad \hat{c}^\dagger_{\mathbf{k}n} = \frac{1}{\sqrt{K\times L}}\sum_{il\alpha}\mathcal{C}^n_{i\alpha}(\mathbf{k})^* e^{-i\mathbf{k}\cdot(\mathbf{R}_l+\mathbf{r}_i)}\,\hat{c}^\dagger_{il\alpha},$$

where n is a band index and $\mathcal{C}^n_{i\alpha}(\mathbf{k})$ are the eigenstate coefficients obtained by a band calculation for a superlattice of L identical clusters. By straightforward substitutions we get

$$\mathcal{G}(\mathbf{k}n\omega) = \frac{1}{K}\sum_{ii'\alpha\beta} e^{-i\mathbf{k}\cdot(\mathbf{r}_i-\mathbf{r}_{i'})}\,\mathcal{C}^n_{i\alpha}(\mathbf{k})^*\mathcal{C}^n_{i'\beta}(\mathbf{k})\,\mathcal{G}_{i\alpha i'\beta}(\mathbf{k}\omega)\,, \tag{7}$$

where $\mathcal{G}_{i\alpha i'\beta}(\mathbf{k}\omega)$ is the superlattice Green function, namely the Fourier transform of the Green function in the local basis

$$\mathcal{G}_{i\alpha i'\beta}(\mathbf{k}\omega) = \frac{1}{L}\sum_{ll'} e^{-i\mathbf{k}\cdot(\mathbf{R}_l-\mathbf{R}_{l'})}\,\mathcal{G}_{\substack{i\alpha i'\beta\\ ll'}}(\omega) \tag{8}$$

and

$$\begin{aligned} \mathcal{G}_{\substack{i\alpha i'\beta\\ ll'}}(\omega) &= \left\langle\Psi_0^N\left|\hat{c}^\dagger_{il\alpha}\left(\hat{G^c}(\omega) + \hat{G^c}(\omega)\hat{V}\hat{G}(\omega)\right)\hat{c}_{i'l'\beta}\right|\Psi_0^N\right\rangle \\ &\quad + \left\langle\Psi_0^N\left|\hat{c}_{il\alpha}\left(\hat{G^c}(\omega) + \hat{G^c}(\omega)\hat{V}\hat{G}(\omega)\right)\hat{c}^\dagger_{i'l'\beta}\right|\Psi_0^N\right\rangle. \end{aligned} \tag{9}$$

All the equations written up to now are exact and approximations are needed in order to make them of practical use. CPT introduces two approximations:

1) $|\Psi_0^N\rangle \sim |\Phi_0^N\rangle$

2) $\sum_m |\Phi_m^{N-1}\rangle\langle\Phi_m^{N-1}| \sim \sum_{il\alpha}\hat{c}_{il\alpha}\,|\Phi_0^N\rangle\langle\Phi_0^N|\,\hat{c}^\dagger_{il\alpha} = 1$
$\sum_m |\Phi_m^{N+1}\rangle\langle\Phi_m^{N+1}| \sim \sum_{il\alpha}\hat{c}^\dagger_{il\alpha}\,|\Phi_0^N\rangle\langle\Phi_0^N|\,\hat{c}_{il\alpha} = 1$

The first one substitutes the unknown ground state $|\Psi_0^N\rangle$ of the full interacting Hamiltonian with $|\Phi_0^N\rangle$, the ground state of $\hat{H}_c$ defined in Eq. (3). As mentioned above, this choice is fairly accurate in the regime of $U/t > 1$ and less correct in the opposite limit. The second assumption corresponds to an approximate expression of the decomposition of unity in terms of a reduced basis for the Fock space of $N \pm 1$ particles.
Altogether we obtain for the total (causal) Green function

$$\begin{aligned}
\underset{ll'}{\mathcal{G}_{i\alpha i'\beta}(\omega)} &= \langle\phi_0^K|\hat{c}_{il\alpha}^\dagger\,\hat{G}^c\,\hat{c}_{i'l'\beta}|\phi_0^K\rangle\,\delta_{ll'} + \langle\phi_0^K|\hat{c}_{il\alpha}\,\hat{G}^c\,\hat{c}_{i'l'\beta}^\dagger|\phi_0^K\rangle\,\delta_{ll'} \\
&\quad + \sum_{l''l'''}\sum_{i''i'''}\sum_{\gamma\gamma'}\Big[\langle\Phi_0^N|\hat{c}_{il\alpha}^\dagger\,\hat{G}^c\,\hat{c}_{i''l''\gamma}|\Phi_0^N\rangle\,\delta_{l''l} + \langle\Phi_0^N|\hat{c}_{il\alpha}\,\hat{G}^c\,\hat{c}_{i''l''\gamma}^\dagger|\Phi_0^N\rangle\,\delta_{l''l}\Big] \\
&\qquad\qquad \times \langle\Phi_0^N|\hat{c}_{i'l''\gamma}^\dagger\,\hat{V}\,\hat{c}_{i'''l'''\gamma'}|\Phi_0^N\rangle\langle\Phi_0^N|\hat{c}_{i'''l'''\gamma'}^\dagger\,\hat{G}\,\hat{c}_{i'l'\beta}|\Phi_0^N\rangle \\
&= \mathcal{G}^c_{i\alpha i'\beta}(\omega)\,\delta_{ll'} \\
&\quad + \sum_{l''l'''}\sum_{i''i'''}\sum_{\gamma\gamma'}\mathcal{G}^c_{i\alpha i'\beta}(\omega)\,\delta_{ll'}\,\langle\Phi_0^N|\hat{c}_{i''l''\gamma}^\dagger\,\hat{V}\,\hat{c}_{i'''l'''\gamma'}|\Phi_0^N\rangle\langle\Phi_0^N|\hat{c}_{i'''l'''\gamma'}^\dagger\,\hat{G}\,\hat{c}_{i'l'\beta}|\Phi_0^N\rangle\,,
\end{aligned} \tag{10}$$

where $\mathcal{G}^c_{i\alpha i'\beta}(\omega) = \langle\Phi_0^N|\hat{c}_{il\alpha}^\dagger\,\hat{G}^c\,\hat{c}_{i'l'\beta}|\Phi_0^N\rangle + \langle\Phi_0^N|\hat{c}_{il\alpha}\,\hat{G}^c\,\hat{c}_{i'l'\beta}^\dagger|\Phi_0^N\rangle$ is the Green function of a disconnected cluster. It is calculated in the Lehmann representation in terms of the few-body states of interacting clusters containing K and $K \pm 1$ electrons

$$\mathcal{G}^c_{i\alpha i'\beta}(\omega) = \sum_n \frac{\langle\phi_0^K|\hat{c}_{i\alpha}^\dagger|\phi_n^{K-1}\rangle\langle\phi_n^{K-1}|\hat{c}_{i'\beta}|\Phi_0^K\rangle}{\omega - (E_0^K - E_n^{K-1})} + \sum_n \frac{\langle\phi_0^K|\hat{c}_{i\alpha}|\phi_n^{K+1}\rangle\langle\phi_n^{K+1}|\hat{c}_{i'\beta}^\dagger|\phi_0^K\rangle}{\omega - (E_n^{K+1} - E_0^K)}. \tag{11}$$

Eq. (10) contains the matrix elements of the inter-cluster potential that are simply calculated identifying the indices $l - l'''$, $i - i'''$, $\gamma - \gamma'$ that give a non-zero contribution.
After summation over the cluster positions in Eq. (8), one eventually reaches an explicit equation for the lattice Green function, namely

$$\mathcal{G}_{i\alpha i'\beta}(\mathbf{k}\omega) = \mathcal{G}^c_{i\alpha i'\beta}(\omega) + \sum_{i'''\gamma'} B_{i\alpha i'''\gamma'}(\mathbf{k}\omega)\,\mathcal{G}_{i'''\gamma' i'\beta}(\mathbf{k}\omega)\,, \tag{12}$$

where the $K \times K$ matrix $B_{i\alpha i'''\gamma'}(\mathbf{k}\omega)$ is the Fourier transform of $\hat{G}^c\hat{V}$ matrix elements involving neighboring sites that belong to different clusters. Eq. (12) is solved by a $K \times K$ matrix inversion at each $\mathbf{k}$ and ω.
The k- and ω-dependent lattice Green function $\mathcal{G}(\mathbf{k}n\omega)$ is obtained by a final summation over the intra-cluster site positions modulated by the single-particle band coefficients as in Eq. (7). The quasi-particle excitation energies correspond to peaks of the k and band-index dependent spectral function

$$A(k, n, \omega) = \operatorname{Im}\mathcal{G}(\mathbf{k}n\omega). \tag{13}$$

Examples of quasi-particle band structure obtained by CPT for model systems are reported in the next section where we start analyzing CPT results for a simplified model system. This analysis will allow us to identify the main features of CPT and to recognize its *pro et contra* with respect to the other many-body approaches. This analysis will constitute a benchmark for CPT and for its application to realistic systems.

3 CPT for model systems

3.1 The role of symmetry

We consider a square 2D lattice with one orbital per site and the standard orbital-independent Hubbard Hamiltonian

$$\begin{aligned} \hat{H}_c &= \sum_{il} \varepsilon_{il}\, \hat{n}_{il} + \sum_{ijl} t_{il,jl}\, \hat{c}^{\dagger}_{il} \hat{c}_{jl} + \sum_{il} U^i\, \hat{n}_{il\uparrow} \hat{n}_{il\downarrow} \\ \hat{V} &= \sum_{ijl \neq l'} t_{il,jl'}\, \hat{c}^{\dagger}_{il} \hat{c}_{jl'} \end{aligned} \tag{14}$$

For this lattice we easily identify various possible "tilings": 4-atom 2×2 square, 4-atom chain, 6-atom rectangle etc. They differ by the number of atoms and also by their symmetry, the 4-atom square being the only one that preserves the full point symmetry of the entire lattice.
The simplest way to check the quality of the main approximation of CPT, the expression of the lattice Green function in terms of Green functions of decoupled clusters, is to look for a convergence in the cluster size, comparing results obtained with larger and larger cluster sizes. This procedure has two serious restrictions that arise i) by the dimensions of Hilbert space used in the exact diagonalization, dimensions that grow exponentially with the number of sites and ii) by symmetry requirements. The second restriction, even if clearly stated in the early developments of Quantum Cluster theories [7], is often overlooked in the implementations. Independently on the various QC *flavors* such as plain CPT [10], variational CPT [13], cellular dynamical mean-field theory [9], the cluster symmetry should be as close as possible to the one of the lattice.
As we know from elementary solid state theory there is a large arbitrariness in the choice of the elementary units that describe a crystalline solid: either the primitive cell that contains the minimum number of atoms, or any larger unit that, via translation invariance, reproduces the crystalline lattice. So the band structure of non-interacting electrons in a 2D square lattice can be calculated using unit cells containing a variable number of atoms, 1, 2, 4, 6, etc., providing exactly the same result, except for a trivial "band folding" that can be easily eliminated by an "unfolding procedure", see Fig. 1.[1]
The situation is quite different for interacting electrons as described by QC theories. In this case the smallest unit must obviously contain more than one atom but its choice is now far less arbitrary since the extended system is described as a periodic repetition of units of correlated electrons and the translation periodicity is preserved only at the superlattice level. In other words, the e-e interaction affects the electronic states inside the cluster, resulting in a sort of hopping renormalization, while the inter-cluster hopping is unaffected. For this reason the cluster symmetry should be as close as possible to the one of the lattice: any significant deviation

[1] The unfolding procedure corresponds to identifying within the bands obtained with a large unit cell those that correspond to the primitive cell. The unfolding procedure is used in CPT in order to implement correctly Eq. (7) where the band index n runs over the number of unfolded bands ($n = 1$ instead of $n = 4$ or $n = 6$ in the present case) but the eigenstates are to be taken in the larger unit cell basis ($i = 1, 4$ or $i = 1, 6$)

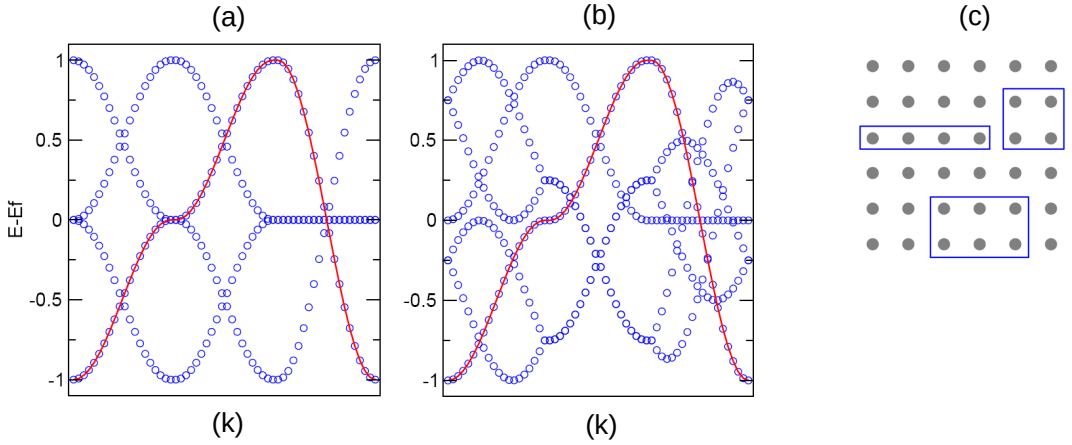

Fig. 1: *Single-particle band structure obtained assuming different unit cells for the 2D square lattice: the 4-site square (a) and the 6-site rectangle (b) (open circles). The red line is the "unfolded" band structure obtained assuming the usual 1-site unit cell. Panel (c) shows different tilings for the 2D square lattice (see text).*

from this requirement would induce a wrong behavior of the quasi-particle band dispersion: quasi-particle energies at k and Rk, R being a point group rotation, would be different, violating a very basic rule of solid state theory.

The influence of cluster symmetry on the quasi-particle band structure is illustrated in Fig. 2 for the square lattice at half occupation. It appears that clusters that are not invariant under lattice point-group rotations give rise to quasi-particle bands that violate the above mentioned rule. Quasi-particle energies should be identical at k-points K_1 and K_2 since K_1 and K_2 are connected by a point-group rotation but for the 4-site chain and the 6-site rectangle they are not, major differences occurring in the first case due to the largest symmetry discrepancies.

Fig. 3 shows a similar comparison for another 2D model system, the honeycomb lattice. In this case two tilings have been considered: the 6-site hexagon and the elongated 8-site cluster. The differences are striking and this is due to the fact that the 8-site tiling has a preferred direction. Hence the dispersions along K–K' and K'–K'' appear different. This result is particularly relevant since it explains some significant discrepancies that are present in the literature on correlated electrons in graphene [14, 15]. In fact, in the honeycomb lattice where the Dirac cones are the consequence of perfect long-range order, theories based on quantum cluster schemes, regardless of them being variational or not and independent on the details of the specific implementations, give rise to a spurious excitation gap for $U \to 0$. A strategy has been proposed that seems to overcome this shortcoming, providing for the undistorted honeycomb lattice a semimetal behavior up to some finite U [16]. The strategy consists in choosing clusters that break the lattice point C_6 symmetry (8- and 10-site clusters). The quasi-particle band dispersion that is obtained in this way presents, however, the above mentioned unphysical behavior which, by the way, is just the origin of the semimetallic behavior at finite U since the gap closes at one K but not at its rotated counterpart. For this reason breaking the rotational symmetry is not an allowed strategy to correct the erroneous insulating phase.

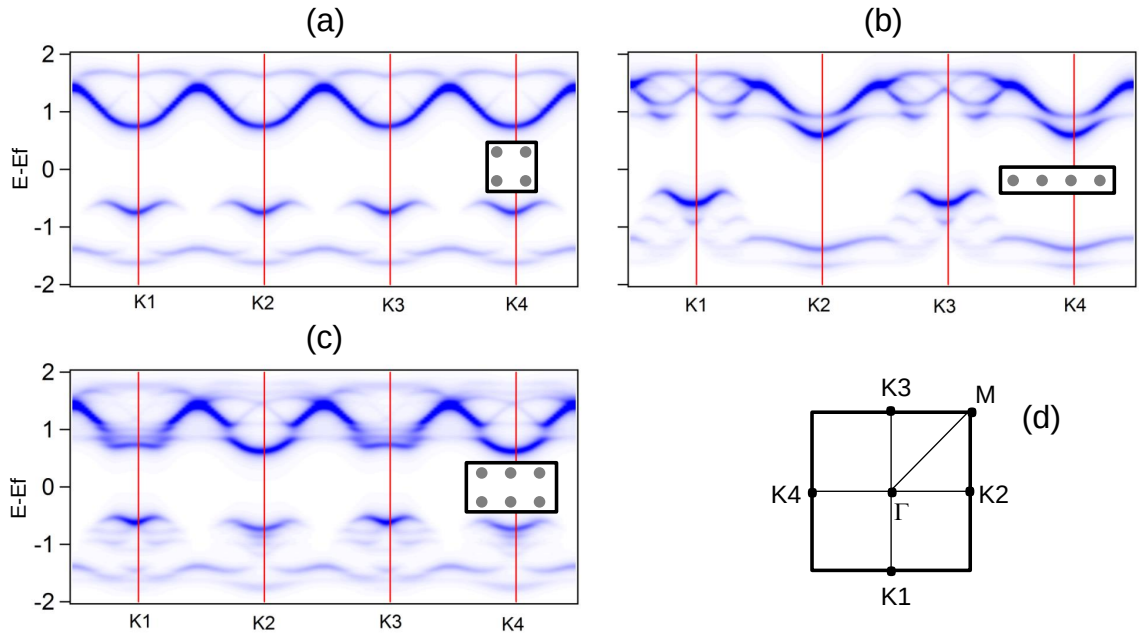

Fig. 2: *Spectral functions obtained for the square lattice at half occupation ($t = 0.25$, $U = 2$) reproduced by different tilings, 4-site square (a), 4-site chain (b) and 6-site rectangle (c). In (d) the 2D square Brillouin Zone is shown.*

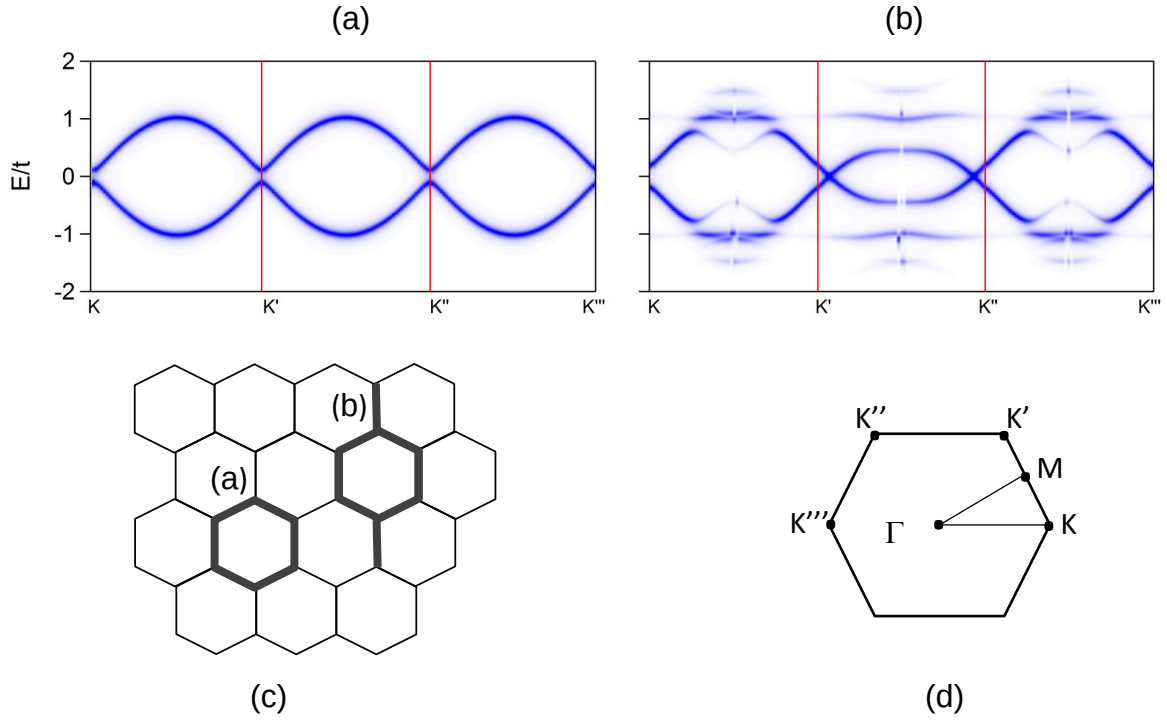

Fig. 3: *Spectral functions obtained for the honeycomb lattice ($t = 1$, $U = 2$) at half occupation using different tilings shown in (c): a 6-site hexagon(a) and an 8-site cluster (b). In (d) the honeycomb Brillouin Zone is shown.*

3.2 CPT vs. other many-body schemes

The agreement between theory and experiments is the ultimate validation of any theoretical scheme. Many-body quasi-particle band structure calculations rely, however, on drastic approximations that may work as *ad-hoc* ingredients that affect the final result: different single-particle band structures are used as a starting point, different strategies are implemented to take into account the double-counting of the e-e interaction, etc. It is then interesting to make a comparison within theory, applying different many-body schemes to the same simplified model. This provides a sort of benchmark for the various theoretical schemes. We choose again the 2D square lattice at half occupation as a paradigmatic case.

Among the non-perturbative techniques that have been proposed to augment band theory by e-e correlations we consider 3-Body Scattering (3BS) theory, a method that shares with other approaches, DMFT above all, the calculation of Green functions in terms of self-energy $\Sigma(\mathbf{k}n\omega)$

$$\mathcal{G}(\mathbf{k}n\omega) = \frac{1}{\omega - e_{\mathbf{k}n} - \Sigma(\mathbf{k}n\omega)}\,, \tag{15}$$

where $e_{\mathbf{k}n}$ are the single-particle band eigenvalues.

In the 3BS approach the interacting many-body state is expanded in the configurations obtained by adding electron-hole pairs to the ground state of the single-particle Hamiltonian. The response of the interacting system to the creation of one hole is then described in terms of interactions between configurations with one hole plus one e-h pair, giving rise to multiple h-h and h-e scattering. The advantage of 3BS with respect to other approaches is to provide a rather intuitive interpretation of the effect of electron correlation on one electron removal energies in terms of Auger-like relaxations. Interestingly, the results of DMFT and 3BS are in many cases quantitatively very similar [4, 17].

The results obtained by 3BS and CPT for the 2D square lattice with $t = 0.25$ and $U = 2, 3, 4$ are shown in Figs. 4 and 5. Both methods provide, for sufficiently large values of U, an insulating behavior but in 3BS the gap opens up only at very large U ($U \geq 2W$) while in CPT the gap is present already at much lower U-values. Indeed, in CPT, at half occupation, the gap is *always* present. It has recently been shown [18] that the existence of a gap down to $U \to 0$ is characteristic of all quantum cluster schemes with the only exception of the dynamical cluster approximation (DCA) [8]. This is due to the aforementioned violation of translational symmetry in quantum cluster methods. DCA preserves translation symmetry and has been shown to describe better the small-U regime; it becomes, however, less accurate at large U values where it overemphasizes the metallic behavior [18]. Aware of this shortcomings we are comparing here results obtained for relatively large U values where CPT limitations are not effective: For $U \gg t$ cluster perturbation theory is expected to provide reliable results.

Other remarkable differences exist between 3BS and CPT results, mainly related to the quasi-particle k-dispersion. This is essentially due to a limitation of the methods based on self-energy calculation, since the self-energy is in most cases assumed k-independent. On the contrary, CPT provides a clear k-dependent energy renormalization and single-particle eigenstates at different k-points are differently affected by e-e correlation. This is shown more clearly by extracting

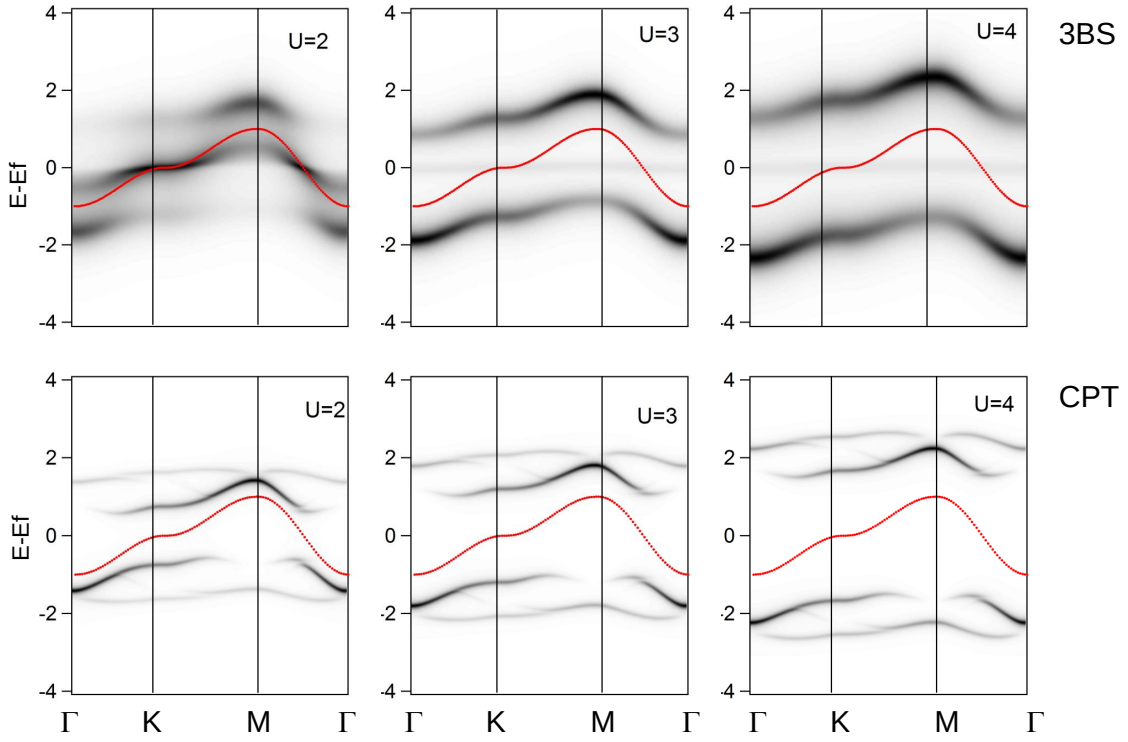

Fig. 4: *Quasi-particle band structure obtained by 3BS (upper panel) and CPT (lower panel) for the 2D square lattice with $t = 0.25$. Increasing values of Hubbard U ($U = 2, 3, 4$) are considered. The k-points are shown in Fig. 2(d).*

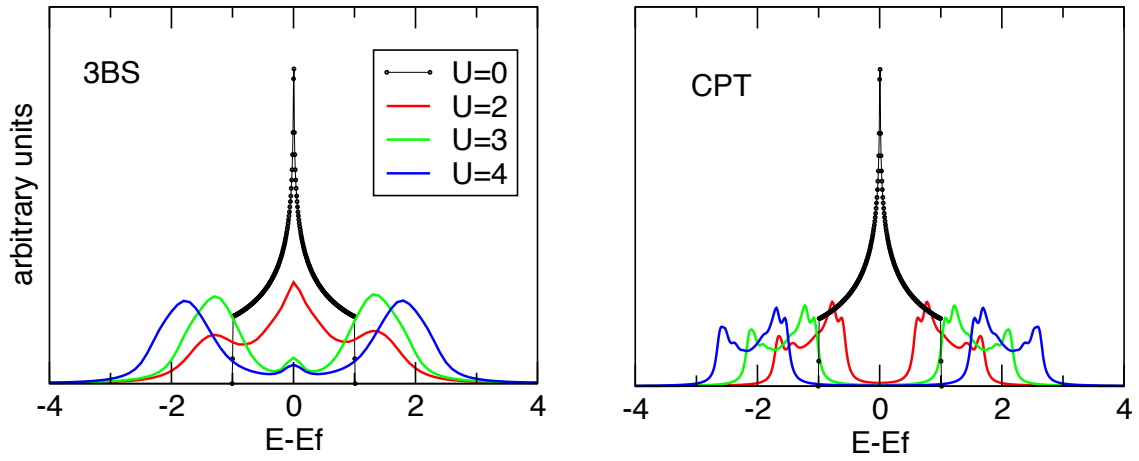

Fig. 5: *Quasi-particle density of states obtained by 3BS (left panel) and CPT (right panel) for the 2D square lattice. Parameter values are the same in Fig. 4.*

from CPT a self-energy

$$\Sigma(\mathbf{k}n\omega) = \omega - e_{\mathbf{k}n} - \mathcal{G}(\mathbf{k}n\omega)^{-1}. \tag{16}$$

CPT self-energies are shown in Fig. 6 at the high symmetry points of the 2D square lattice showing a well defined k-dependence.

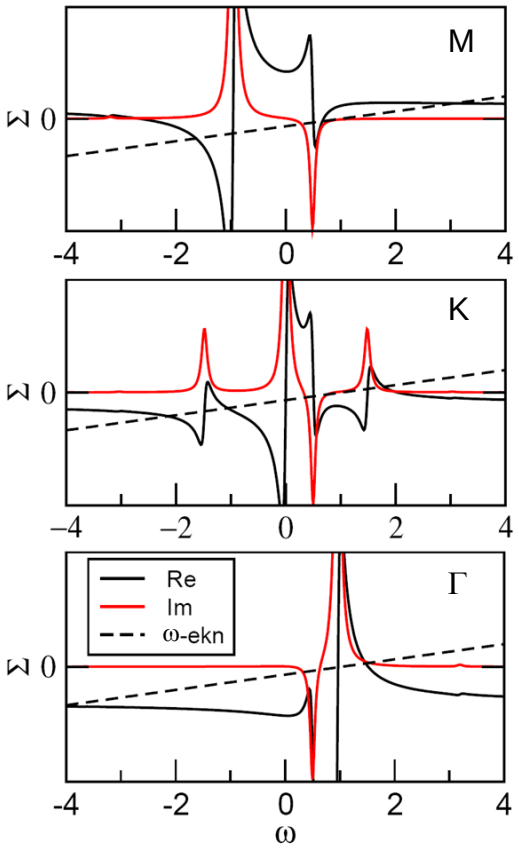

Fig. 6: *k-dependent CPT self-energy for the 2D square lattice. Parameters as in Fig. 4.*

4 Transition-metal oxides

4.1 Preliminaries

We move now to Transition Metal (TM) oxides as an example of the application of CPT to real materials.

The non interacting contribution to the Hubbard Hamiltonian is a standard Tight-Binding (TB) Hamiltonian that can be written in terms of Koster-Slater parameters obtained by fitting ab-initio band structure. Tables 1 and 2 report the Koster-Slater tight-binding parameters of the $3d$ transition-metal oxides obtained by least squares fitting of ab-initio band structures calculated in the DFT-LMTO scheme.

When using TB parameters in the Hubbard Hamiltonian we must take care of the double-counting issue: the ab-initio band structures, and the TB parameters deduced from it, contain the e-e Coulomb repulsion as a mean-field that must be removed before including U as a true many-body term. "Bare" on-site parameters are calculated by subtracting the mean filed value of the Hubbard term, namely

$$E^*_\alpha = E_\alpha - \sum_i U^i_\alpha \langle n_{i\alpha\uparrow}\rangle \langle n_{i\alpha\downarrow}\rangle \,. \tag{17}$$

This definition involves the d occupation inside the cluster that is actually used in exact diagonalization and cancels out the energy shift due to double counting within each sub-cluster. Other

Table 1: *On-site Koster-Slater parameters (in eV).*

	$E_s(TM)$	$E_p(TM)$	$E_{t2g}(TM)$	$E_{eg}(TM)$	$E_s(O)$	$E_p(O)$
MnO	7.313	11.546	-0.763	-0.010	-18.553	-4.806
FeO	8.208	12.232	-0.857	-0.132	-18.489	-4.723
CoO	8.221	12.040	-1.383	-0.734	-18.673	-4.891
NiO	8.6332	12.176	-1.767	-1.165	-18.608	-4.806

Table 2: *Inter-site Koster-Slater parameters (in eV).*

atom	atom	ss_σ	pp_σ	pp_π	dd_σ	dd_π	dd_δ	sp_σ	sd_σ	pd_σ	pd_π
Mn	Mn	-0.514	1.435	-0.137	-0.353	0.028	0.047	0.486	-0.285	-0.081	0.209
O	Mn	0.0	0.0	0.0	0.0	0.0	0.0	0.0	-1.074	-1.243	0.632
O	O	-0.124	0.519	-0.102	0.0	0.0	0.0	-0.016	0.0	0.0	0.0
Fe	Fe	-0.529	1.470	-0.128	-0.341	0.023	0.046	0.487	-0.275	-0.083	0.195
O	Fe	0.0	0.0	0.0	0.0	0.0	0.0	0.0	-1.083	-1.027	0.640
O	O	-0.140	0.578	-0.109	0.0	0.0	0.0	-0.015	0.0	0.0	0.0
Co	Co	-0.537	1.497	-0.109	-0.306	0.015	0.045	0.483	-0.283	-0.123	0.193
O	Co	0.0	0.0	0.0	0.0	0.0	0.0	0.0	-1.023	-1.235	0.616
O	O	-0.145	0.609	-0.112	0.0	0.0	0.0	-0.043	0.0	0.0	0.0
Ni	Ni	-0.549	1.527	-0.090	-0.280	0.006	0.043	0.488	-0.294	-0.113	0.189
O	Ni	0.0	0.0	0.0	0.0	0.0	0.0	0.0	-0.969	-1.209	0.608
O	O	-0.154	0.656	-0.116	0.0	0.0	0.0	-0.101	0.0	0.0	0.0

Table 3: d*-orbital occupations.*

	MnO	FeO	CoO	NiO
n_{t2g}	4.941	5.770	5.961	5.966
n_{eg}	0.599	0.672	1.614	2.556
n_d	5.540	6.441	7.575	8.522

definitions of double-counting correction have been proposed in the spirit of LDA+U [12] that involve the average d-occupation in the solid calculated by single-particle theory. Our choice should be preferred when using multiple partitions of sites/orbitals: this double-counting correction in fact amounts to readjusting the "center of mass" of the calculated few-particle states by realigning the calculated $\frac{1}{2}(E_0^{N+1} - E_0^{N-1})$ to its $U = 0$ value and to keep the distinction between filled and empty states.

Fig. 7 reports the local density of states obtained in the non-interacting scheme. We focus in particular on the TM d-orbital contribution. Crystal field symmetry induces a split of d-orbitals into t_{2g}/e_g-states and according to ab-initio band theory these states have different occupations (see Table 3). This is a crucial point that will be exploited later in applying CPT to TM oxides.

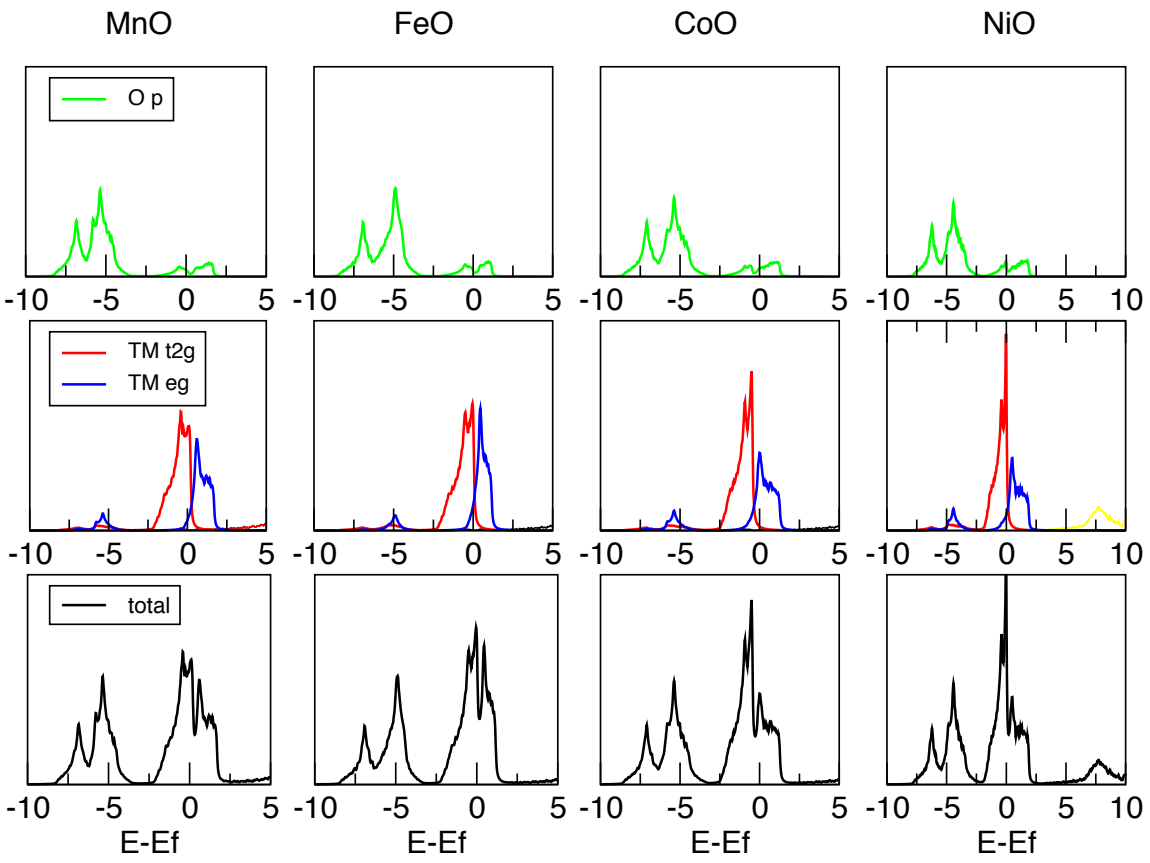

Fig. 7: *Single-particle Density of States (DOS) for TM oxides of the* $3d$ *series. The total DOS is reported (lower panel) together with the contributions of TM d-orbital (in red and blue* t_{2g} *and* e_g*, respectively) and of oxygen* sp*-orbitals in the upper panels.*

4.2 Lattice tiling: a multiple partition strategy

As outlined in the previous sections, the first step of the CPT procedure is the partitioning of the lattice into clusters. Obviously the choice in not unique but must satisfy some requirements: the clusters should be connected by inter-site hopping as schematically indicated in Fig. 8(c), namely they should not overlap; moreover they should contain enough atoms to include the relevant physics of the interacting system and finally the number of sites/orbitals per cluster should be tractable in an exact diagonalization procedure. Another relevant criterion is that, as discussed in Section 3, the cluster symmetry should be as close as possible to the lattice one.

TM oxides of the $3d$ series (MnO, NiO, CoO, FeO) crystallize in the rocksalt structure. An octahedral cluster containing one TM atom and 6 nearest-neighbor oxygens has been originally proposed as the elementary unit containing all the relevant physics of the system; atomic multiplet theory applied to this isolated cluster [19] has been used to reproduce some features of the solid state system, losing, however, the translational symmetry and all k-related quantities. The same cluster has been used as the basic unit to be embedded in an infinite medium in the spirit of variational CPT [12]. These clusters, however, do overlap in the rocksalt structure and cannot be used as elementary unit in CPT calculations. Moreover this cluster contains just one TM atom and even in variational CPT the resulting self-energy turns out to be k-independent [12].

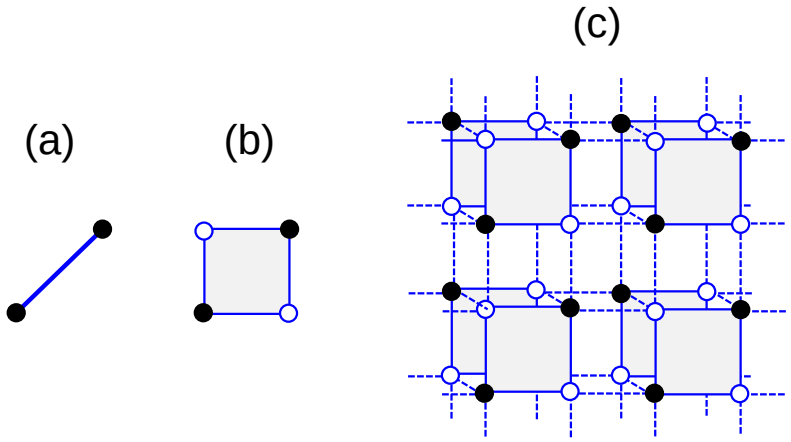

Fig. 8: *Building blocks of the 3D Rocksalt structure for a transition-metal mono-oxide: (a) a dimer of 2 TM atoms (filled black circles); (b) a* 2×2 *plaquette containing the two atomic species (oxygens as open circles); (c) stacking of plaquette layers reproducing the 3D lattice. Dotted lines indicate the inter-cluster hopping.*

The smallest cluster containing more than one TM atom and reproducing, without overlaps, the 3D rocksalt lattice is the 2×2 plaquette of Fig. 8(b) with two TM atoms and two oxygens. Since the bands of TM oxides around the Fermi energy are described by 9 spd-orbitals for each TM atom and 4 sp-orbitals for each oxygen, the dimension of the Hilbert space spanned by the Slater determinants that are obtained by populating in all possible ways the $K = 26$ orbitals with P electrons of a given spin ($P = 13 \ldots 16$ from MnO to NiO) is far too big (number of configurations $= (\frac{K!}{P!(K-P)!})^2$) for exact diagonalization.
A reduction of the number of sites/orbitals per cluster is mandatory. To this end we may identify, within a single cluster, two classes of orbitals (centered on different sites and of different symmetry) that we call A and B; we may then write the cluster Hamiltonian as the sum of on-site and inter-site terms connecting all kinds of orbitals: A-A, B-B (diagonal terms), and A-B (off-diagonal terms):

$$\hat{H}_c \;=\; \hat{H}^{\rm diag} + \hat{V}_{AB} \tag{18}$$

with

$$\hat{H}^{\rm diag} = \hat{H}_c^{AA} + \hat{H}_c^{BB} \quad \text{and} \quad \hat{V}_{AB} = \sum_{\alpha_A \beta_B} t_{il\alpha_A, jl\beta_B}\, \hat{c}^{\dagger}_{il\alpha_A} \hat{c}_{jl'\beta_B}\,. \tag{19}$$

Here

$$\hat{H}_c^{AA} = \sum_{il\alpha_A} \varepsilon_{il\alpha_A}\, \hat{n}_{il\alpha_A} + \sum_{\alpha_A \beta_A} \sum_{ijl} t_{il\alpha_A, jl\beta_A}\, \hat{c}^{\dagger}_{il\alpha_A} \hat{c}_{jl\beta_A} + \sum_{il\alpha_A\beta_A} U^{i}_{\alpha_A\beta_A}\, \hat{n}_{il\alpha_A\uparrow} \hat{n}_{il\beta_A\downarrow} \tag{20}$$

and a similar expression for $\hat{H}_c^{BB}$.
Correspondingly we have again $\hat{G^c}^{-1} = z - \hat{H}_c = (\hat{G}^{\rm diag})^{-1} - \hat{V}_{AB}$ which results, as before, in a Dyson-like equation

$$\hat{G^c} = \hat{G}^{\rm diag} + \hat{G}^{\rm diag}\, \hat{V}_{AB}\, \hat{G^c}\,. \tag{21}$$

In the local basis $\hat{G}^{\rm diag}$ is block-diagonal and the non-zero elements $\hat{G}^{diag}_{AA}$ and $\hat{G}^{\rm diag}_{BB}$ are obtained by performing separate exact diagonalizations that include either A or B orbitals. In this basis Eq. (21) can be solved by matrix inversion.

$$\hat{G}^c = (\mathbb{I} - \hat{G}^{\rm diag}\,\hat{V}_{AB})^{-1}\,\hat{G}^{\rm diag} \tag{22}$$

with $\mathbb{I}$ the unit matrix and indices running over the $K = 26$ sites/orbitals of the plaquette (9 spd-orbitals on 2 TM atoms and 4 sp-orbitals on 2 oxygens). More explicitly

$$\begin{pmatrix} G_{AA} \\ G_{AB} \\ G_{BA} \\ G_{BB} \end{pmatrix} = \begin{pmatrix} 1 & 0 & -G^{\rm diag}_{AA}\,V_{AB} & 0 \\ 0 & 1 & 0 & -G^{\rm diag}_{AA}\,V_{AB} \\ -G^{\rm diag}_{BB}\,V_{BA} & 0 & 1 & 0 \\ 0 & -G^{\rm diag}_{BB}\,V_{BA} & 0 & 1 \end{pmatrix}^{-1} \begin{pmatrix} G^{\rm diag}_{AA} \\ 0 \\ 0 \\ G^{\rm diag}_{BB} \end{pmatrix}. \tag{23}$$

Of course this multiple partition – within the lattice and within the cluster – makes the problem numerically tractable. In this case the CPT prescriptions may be rephrased as follows: chose a partitioning of the lattice Hamiltonian into a set of non-overlapping clusters connected by inter-cluster hopping; make a further partition inside each cluster defining a suitable collection of sites/orbitals; perform separate exact diagonalizations plus matrix inversion to calculate the cluster Green function in the local basis by Eq. (23) and finally obtain the full lattice Green function in the Bloch basis by Eq. (12).

This technique can be extended to more than two subsets of sites/orbitals, and, in fact, we have applied it to a triple partition (subsets A, B and C) as we will show in more detail below. It has the advantage to replace an unmanageable exact diagonalization with two (or more) separate ones followed by a matrix inversion. It shares with CPT the assumption about the states of the *cluster* interacting electrons $\phi^K(r_1, r_2.., r_K) \sim \phi_A(r_1, r_2.., r_A)\phi_B(r_1, r_2.., r_B)...$ This is a drastic approximation whose validity must be verified performing calculations with different partitions and/or finding explicit and justified rules for the adopted choice. These rules must be based on clear and sound conjectures and will be inevitably system-dependent.

4.3 Multiple partition for TM oxides

We come now to the practical implementation appropriate for transition-metal oxides. TM oxides of the $3d$ series differ drastically in d-band occupation; according to single-particle band theory reported in Tab. 3 and Fig. 7, NiO and CoO have t_{2g}-states fully occupied ($n_{t2g} \simeq 6$ in both cases) while the e_g-states are responsible for the metallic behavior; on the contrary, in MnO and FeO both t_{2g}- and e_g-states cross the Fermi level. Since only partially occupied shells are affected by the e-e interaction this suggests different partitions for the two classes of TM oxides, NiO, CoO on one side (with only e_g-orbitals centered on the two TM atoms in the plaquette) and FeO, MnO on the other site (with both t_{2g}-e_g-orbitals).

Once we have made this assumption we are also able to predict straightaway which TM oxide will develop in CPT a Mott-Hubbard gap: in exact diagonalization, in fact, only systems at half occupation exhibit a finite energy separation between hole and particle excitations and

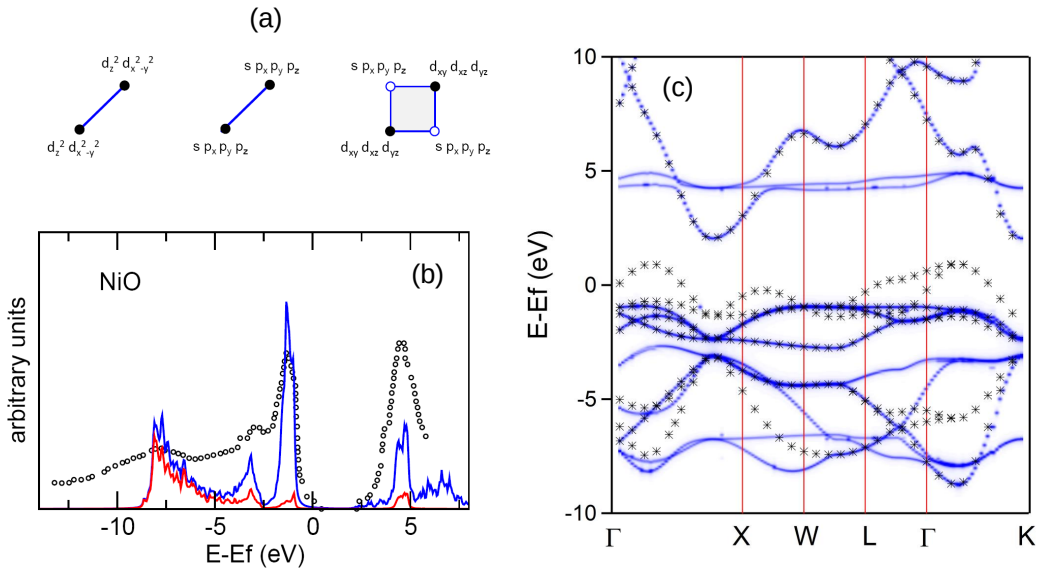

Fig. 9: *CPT results for NiO assuming the multiple partition indicated in (a) (see text). (b): orbital resolved density of quasi-particle states compared with experimental results (open circles). Blue (red) line is for TM d (Oxygen sp) orbital contribution. (c): Quasi-particle band dispersion (blue line) compared with the single-particle result (black asterisks).*

we expect NiO and MnO (having 2 e_g and 5 t_{2g}-e_g electrons respectively) to be well-defined Mott insulators, while in FeO and CoO, where both t_{2g} and e_g are not half occupied, local e-e repulsion is expected to induce a readjustment of spectral weight but not necessarily a well defined gap. In the following we will describe how CPT can be implemented to capture gap opening in MnO and NiO.

The multiple-partition–multiple-embedding procedure for NiO starts from a separation of Ni-d orbitals into t_{2g} and e_g contributions. As already mentioned, in NiO only e_g-states are partially occupied and it is reasonable to expect them to be most affected by e-e interaction. We identify the set of finite systems shown in Fig. 9(a), namely: i) a Ni dimer containing e_g orbitals, ii) a Ni dimer containing sp-orbitals, iii) a 4-atom plaquette with Ni t_{2g}- and O sp-orbitals. Three distinct exact diagonalizations are performed assuming for simplicity non-zero on-site repulsion between Ni d-orbitals only. Three cluster Green functions are calculated within the Lehmann representation: G_{AA}, G_{BB}, and G_{CC} with $A \equiv$ Ni e_g, $B \equiv$ Ni sp, and $C \equiv$ O p Ni t_{2g}. The total Green function for the plaquette is obtained by putting them together. This is the first embedding procedure and amounts to solving the matrix equation (23) extended to a triple-partition.

The second embedding procedure corresponds to going from the 2×2 plaquette to the extended lattice and requires the kind of "periodization" described in Sec. 2, where we go from the cluster Green function to the lattice Green function by solving again the Dyson-like equation involving now inter-cluster interactions. In order to implement Eq. (12) one needs first of all to define for each site $r_{i'}$ in the plaquette the position of the nearest neighbors $\mathbf{r}_{i''}$ and the corresponding lattice vectors $\mathbf{R}_{l''}$ connecting the cluster with the neighboring ones. Then the matrix $B_{i\alpha j\gamma}(\mathbf{k}\omega)$ is obtained as follows

$$B_{i\alpha j\gamma}(\mathbf{k}\omega) = \sum_{i'i''l''} t_{i'0\alpha i''l''\gamma}\, e^{-i\mathbf{k}\cdot\mathbf{R}_{l''}}\, \mathcal{G}^{c}{}_{i\alpha i'\gamma}(\omega)\, \delta_{i''j}\,. \tag{24}$$

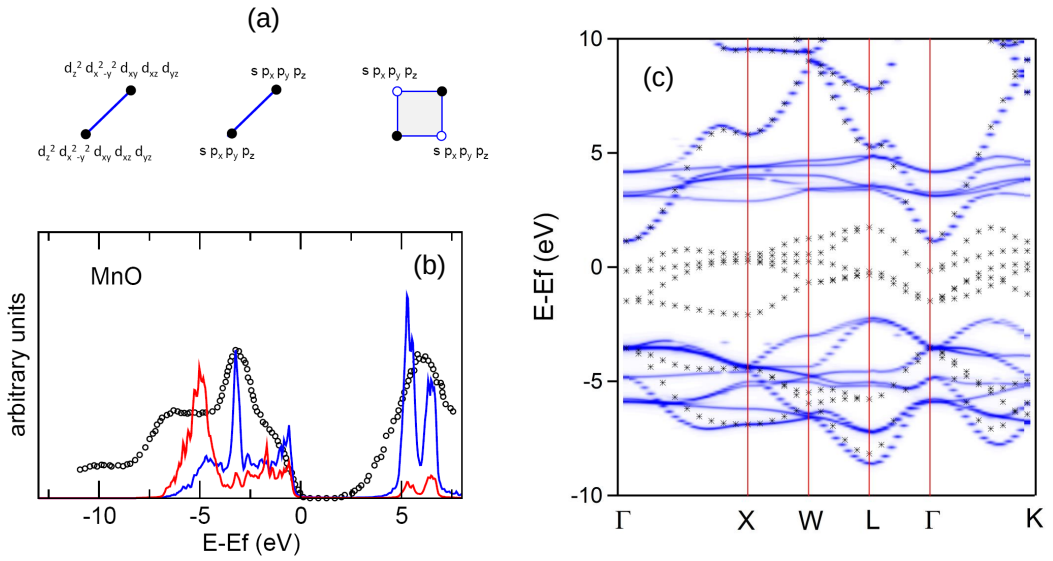

Fig. 10: *CPT results for MnO. (a): multiple partition of orbitals in dimer and* 2×2 *plaquette (see text). (b): orbital resolved density of quasi-particle states compared with the experimental data (circles). Blue (red) line is for TM* d *(Oxygen* sp*) orbital contribution. (c): quasi-particle band dispersion (blue line) compared with the single-particle result (black asterisks).*

Here $t_{i'0\alpha i''l''\gamma}$ are the inter-site hopping terms previously defined (Eq. (2)) obtained in terms of Koster-Slater parameters in the usual way.

The on-site e-e interaction involving Ni d-orbitals has the effect of opening a gap between t_{2g}-states as expected and to turn the NiO into a wide-gap insulator. The Hubbard U is used here as a tunable parameter to reproduce the experimental gap but its value ($U = 11$ eV) is within the current estimates. We notice that, in spite of the drastic approximations, the agreement between theory and experiment is quite good, not only for the correct gap that is somewhat fixed by the value of the e-e repulsion, but also for the orbital character of the valence-band edge, largely involving O $2p$-states as known from experiments.

Let us consider now MnO where, according to the previous discussion, we include in the smallest elementary unit (the dimer) all d electrons (Fig. 10(a)). Then also in this case we will be dealing with an exact diagonalization at half occupation. The dimension of the Hilbert space spanned by the Slater determinants is here $n_{\rm conf} = (\frac{K!}{P!(K-P)!})^2 = 63\,504$, so large to require the band-Lanczos algorithm to obtain ~ 1000 eigenvalues and eigenvectors $E_n^{N\pm1}$, $\Phi_n^{N\pm1}$ for the system with $N \pm 1$ electrons as well as the ground state E_n^N, Φ_0^N for the N electron system. Also in this case the dimer problem accounts for both hopping and e-e repulsion on the d-orbitals of the TM atoms and therefore includes a large part of the relevant physics of the interacting system. In particular, since also in this case the system is half occupied, we expect the ground state E_0^{N+1} to be larger than E_0^{N-1} with an energy distance growing with U. This is essential in view of a gap opening in the extended system.

We then proceed as before to *embed* first the dimer into the plaquette and finally the plaquette into the extended lattice. Results are shown in Fig. 10. In this case the e-e repulsion is responsible for a complete removal of all Mn d-states around the Fermi level as required for the gap opening.

Figure 10(b) shows a comparison between the quasi-particle density of states and the experimental results of Ref. [20]. We observe that the gap value is well reproduced as well as most of the spectroscopic structures. We do not find evidence of structures below the valence-band bottom that are observed in photoemission experiments; this might be due to the reduced number of excited states that are obtained by the Lanczos procedure. We mention however that the origin of satellite features in MnO has been somewhat controversial in the literature attributing them either to intrinsic [20] or extrinsic effects [21]. Apart from the satellite structure our results are comparable with what has been obtained by variational cluster approximation [12] in spite of a different choice of the cluster, and by a recent DMFT calculations [22]. Since these two approaches are either variationally optimized or self-consistent, we may identify in the present CPT scheme the advantage of giving comparable results by a single-shot calculation thanks, we believe, to our cluster choice.

5 Concluding remarks

In this lecture we have reviewed a possible strategy, based on a multi-orbital extension of the CPT approach, to include on-site e-e interactions in real materials and we have discussed its application to the paradigmatic case of transition-metal oxides. The CPT strategy is applied twice, first to identify a partition of the lattice into non overlapping clusters and secondly to calculate the cluster Green function in terms of two or more local ones. This procedure has the advantage of replacing an unmanageable exact diagonalization by two or more separate ones followed by a matrix inversion. This strategy may be adopted whenever dealing with exceedingly large dimensions of the configuration space, for instance in treating correlated electrons in low-dimensional systems such as surfaces and interfaces, where the translation invariance is reduced and the unit cell contains many atoms. Of course there are drastic approximations involved: in the same way as in the standard single-orbital CPT, writing the lattice Green function in terms of Green functions of decoupled subunits amounts to identifying the many-electron states of the extended lattice as the product of cluster few-electron states. In the present case in particular, choosing the TM dimer as the basic unit we have excluded from the few-electron eigenstates obtained by exact diagonalization the contribution of oxygen sp-orbitals, treating the O sp – TM d hybridization by the embedding procedure. The non-interacting part of the lattice Hamiltonian is described in terms tight-binding parameters deduced by a least-squares fitting of an ab-initio single-particle band structure, including all the relevant orbitals. To our purposes, since we do not need any real-space expression of the single-particle wavefunctions, this tight-binding parametrization is fully equivalent to a representation in terms of maximally localized Wannier functions. We have applied this method to NiO and MnO as test cases and, using a single value of the Hubbard U, we have found a reasonable agreement with experimental data and with theoretical results obtained by different methods.

References

[1] G. Kotliar, S.Y. Savrasov, K. Haule, V.S. Oudovenko, O. Parcollet, and C.A. Marianetti, Rev. Mod. Phys. **78**, 865 (2006)

[2] F. Manghi, C. Calandra, and S. Ossicini, Phys. Rev. Lett. **73**, 3129 (1994)

[3] S. Monastra, F. Manghi, C.A. Rozzi, C. Arcangeli, E. Wetli, H.-J. Neff, T. Greber, and J. Osterwalder, Phys. Rev. Lett. **88**, 236402 (2002)

[4] J. Sánchez-Barriga, J. Fink, V. Boni, I. Di Marco, J. Braun, J. Minár, A. Varykhalov, O. Rader, V. Bellini, F. Manghi, H. Ebert, M.I. Katsnelson, A.I. Lichtenstein, O. Eriksson, W. Eberhardt, and H.A. Dürr, Phys. Rev. Lett. **103**, 267203 (2009)

[5] J. Sánchez-Barriga, J. Minár, J. Braun, A. Varykhalov, V. Boni, I. Di Marco, O. Rader, V. Bellini, F. Manghi, H. Ebert, M.I. Katsnelson, A.I. Lichtenstein, O. Eriksson, W. Eberhardt, H.A. Dürr, and J. Fink, Phys. Rev. B **82**, 104414 (2010)

[6] J. Sánchez-Barriga, J. Braun, J. Minár, I. Di Marco, A. Varykhalov, O. Rader, V. Boni, V. Bellini, F. Manghi, H. Ebert, M.I. Katsnelson, A.I. Lichtenstein, O. Eriksson, W. Eberhardt, H.A. Dürr, and J. Fink, Phys. Rev. B **85**, 205109 (2012)

[7] T. Maier, M. Jarrell, T. Pruschke, and M.H. Hettler, Rev. Mod. Phys. **77**, 1027 (2005)

[8] M.H. Hettler, A.N. Tahvildar-Zadeh, M. Jarrell, T. Pruschke, and H.R. Krishnamurthy, Phys. Rev. B **58**, R7475 (1998)

[9] G. Kotliar, S.Y. Savrasov, G. Pálsson, and G. Biroli, Phys. Rev. Lett. **87**, 186401 (2001)

[10] D. Sénéchal, D. Perez, and M. Pioro-Ladrière, Phys. Rev. Lett. **84**, 522 (2000)

[11] F. Manghi, J. Phys.: Condens. Matter **26**, 015602 (2014)

[12] R. Eder, Phys. Rev. B **78**, 115111 (2008)

[13] M. Potthoff, M. Aichhorn, and C. Dahnken, Phys. Rev. Lett. **91**, 206402 (2003)

[14] F. Grandi, F. Manghi, O. Corradini, and C.M. Bertoni, Phys. Rev. B **91**, 115112 (2015)

[15] F. Grandi, F. Manghi, O. Corradini, C.M. Bertoni, and A. Bonini, New J. Phys. **17**, 023004 (2015)

[16] M. Laubach, J. Reuther, R. Thomale, and S. Rachel, Phys. Rev. B **90**, 165136 (2014)

[17] F. Manghi and V. Boni, Journal of Electron Spectroscopy and Related Phenomena **200**, 181 (2015)

[18] A. Liebsch and W. Wu, Phys. Rev. B **87**, 205127 (2013)

[19] A. Fujimori, K. Terakura, M. Taniguchi, S. Ogawa, S. Suga, M. Matoba, and S. Anzai, Phys. Rev. B **37**, 3109 (1988)

[20] J. van Elp, R.H. Potze, H. Eskes, R. Berger, and G.A. Sawatzky, Phys. Rev. B **44**, 1530 (1991)

[21] A. Fujimori, N. Kimizuka, T. Akahane, T. Chiba, S. Kimura, F. Minami, K. Siratori, M. Taniguchi, S. Ogawa, and S. Suga, Phys. Rev. B **42**, 7580 (1990)

[22] P. Thunström, I. Di Marco, and O. Eriksson, Phys. Rev. Lett. **109**, 186401 (2012)